Proceedings of ASME Turbo Expo 2014: Turbine Technical Conference and Exposition
GT2014
June 16 – 20, 2014, Düsseldorf, Germany

GT2014-25977

VALIDATION RESULTS FOR A DIVERSE SET OF TURBOMACHINERY CASES USING A DENSITY-BASED OpenFOAM® SOLVER

Mark R. Anderson
IntegralX Incorporated
Norwich, VT USA

Daryl L. Bonhaus
Concepts NREC
White River Junction, VT USA

ABSTRACT

A validation study of a variety of compressible flow turbomachinery cases is presented with comparisons to test data using OpenFOAM. OpenFOAM is open-source code consisting of various solvers and computational libraries focused on CFD. The study used a particular solver version with a density based approach that was derived from the "extended" branch of OpenFOAM. The example cases all consisted of single blade row designs at steady state and were run fully viscous (unless noted otherwise) with various turbulence models.

The results showed a definite superiority of the density based solver over other OpenFOAM solvers in a test suite of simplified cases as well as in more complex examples in actual turbomachinery designs. A typical Laval nozzle case and transonic bump case are presented demonstrating the basic ability of the solver to capture shocks and to handle transonic flow in general. Actual turbomachinery applications consisted of a two-dimensional transonic compressor cascade, a moderately supersonic two-dimensional turbine cascade, two radial compressor cases, and a radial inflow turbine.

The results showed the solver to be very capable of capturing pressure distributions and, most importantly, aerodynamic loss through the machines. The ability of the solver to accurately model performance in a wide range of different designs and across the entire performance map was demonstrated. Detailed comparisons to highly regarded test data are shown.

Special examination was made of the computational costs of the solver which were quite high with run times coming in at about 10 times longer than other commercial compressible flow solvers. Several acceleration methods are discussed which significantly improved run time performance.

INTRODUCTION

OpenFOAM[1] is an open-source library of finite volume solution methods and utilities that are distributed with various CFD solvers for different classes of flow conditions. Several variations of OpenFOAM are available, the two most significant being: the original branch first released in open source in 2004 (1, 2) and the "Extend Project" branch (3, 4). Beyond these two major branches are many sub-branches and projects generally related to solving more specific problem sets. Of particular importance to compressible flow turbomachinery is a density-based solver by Borm *et al*. (5, 6) which is available as a special project off of the extended branch. The critical feature of this solver is that it is a density based approach which uses a Godunov flux method combined with a Riemann solver. Other special accommodations specific for turbomachinery are included as well (7, 8). All the results shown in this paper, unless specifically labeled otherwise, were produced from this solver. This paper is a continuation of validation work previously presented by the first author (9).

The validation study reviewed in this paper is an attempt to examine a statistically significant number of compressible flow turbomachinery examples using the best available variation of OpenFOAM. The study used well documented test data (10) from a variety of sources. A hierarchal approach was used, starting with simple cases to determine viability of the solver for compressible flow, two-dimensional turbomachinery cascades, and finishing with full three-dimensional turbomachinery examples. Unless otherwise stated, all cases were run fully turbulent assuming periodicity of each flow passage and steady-state.

[1] OpenFOAM is a registered trademark of OpenCFD Limited.

As a basis of comparison, the OpenFOAM solver results are compared to the Pushbutton CFD®[2] code (11, 12). Pushbutton CFD is very well validated and widely used in the turbomachinery industry. Each of the cases shown used the same grid, equation of state, and turbulence model selection (not necessarily the same implementation) for both solvers. Comparison to another solver gives valuable insights into the results and helps to indicate when the errors are the direct result of solver deficiencies or merely represent inherent limits in the turbulence model, grid resolution, test error, or even setup and interpretation.

The OpenFOAM solutions were generally run with settings consistent with the example cases included in the density based solver branch. A variety of turbulence models were used and are stated individually for each case. All solutions were advanced using 4th order Runge-Kutta time stepping. The default van Albada limiter was set with the HLLC ALE Riemann solver for all cases. Local time stepping was used and a CFL of 1.0 was most typical.

CONVERGING/DIVERGING NOZZLE

The first example shown is a simple converging/diverging nozzle (also called a Laval nozzle). The long length scale in the stream-wise direction gives the flow a quasi-one-dimensional characteristic. Despite its geometric simplicity, it provides a challenging example for compressible flow solvers and for shock capturing in particular.

Figure 1 shows the results for low supersonic flow condition for three solvers. Pushbutton CFD (blue), OpenFOAM: *rhoSimplecFoam* (green), and OpenFOAM: *transonicMRFDyMFoam* (red). All solutions were run Euler on a 2 dimensional mesh. The results show the failure of the compressible pressure-based solver *rhoSimpleFoam* to capture the transonic nature of the flow. In contrast, the density-based *transonicMRFDyMFoam* provides a virtually identical result to Pushbutton CFD including the tight shock capturing. The results clearly show the superiority of the density-based solver over other OpenFOAM solvers, almost all of them pressure-based. All further results quoted from OpenFOAM in this paper will be from the *transonicMRFDyMFoam* solver.

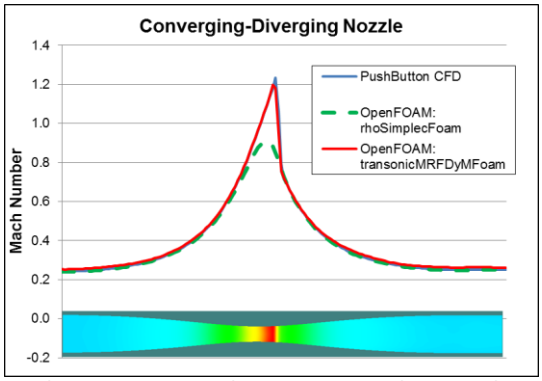

Figure 1. CENTERLINE MACH NUMBER FOR A MODERATELY SUPERSONIC CONVERGING AND DIVERGING NOZZLE.

[2] Pushbutton CFD is a registered trademark of Concepts ETI, Inc.

Figure 2 shows a higher Mach number flow peaking at over 1.6 which is about as high as is seen in turbomachinery in all but the most specialized designs. The results show very close agreement at this high speed condition as well.

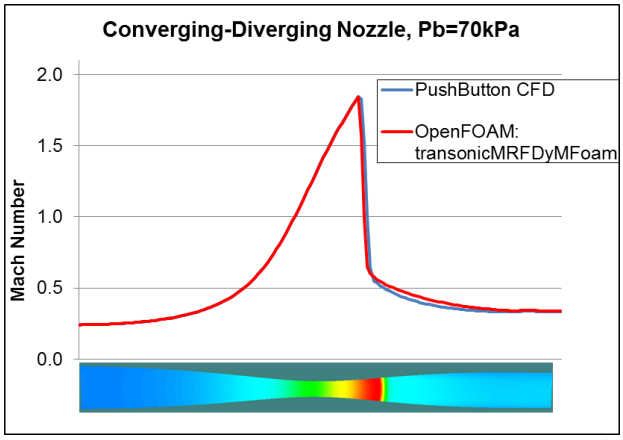

Figure 2. CENTERLINE MACH NUMBER FOR A HIGHLY SUPERSONIC CONVERGING AND DIVERGING NOZZLE

TRANSONIC BUMP

The transonic bump is a well-known case often used to determine the viability of compressible flow solvers (13). At its simplest, it demonstrates how a simple geometry can generate transonic flow with a shock. Figure 3 shows the Mach number distribution for both Pushbutton CFD (top) and OpenFOAM (bottom) both run in inviscid Euler mode. The results show very close agreement in the false color Mach number plot. Figure 4 also shows excellent agreement between the two solvers in terms of surface pressure distributions.

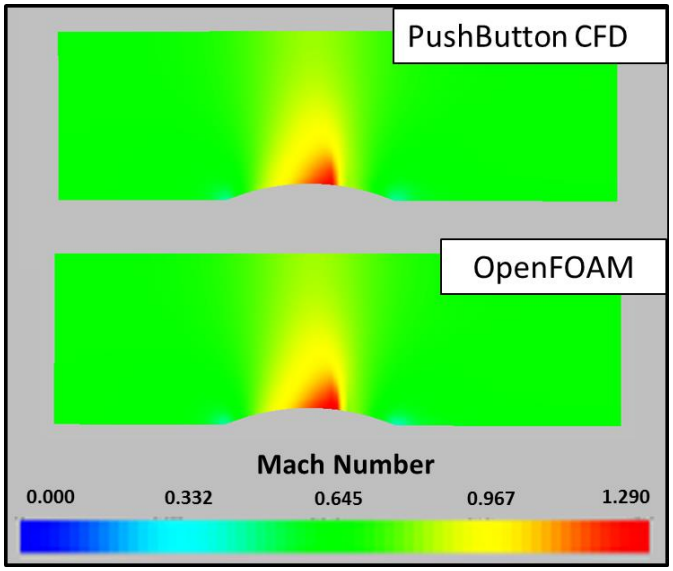

Figure 3. EULER MACH NUMBER DISTRIBUTIONS FOR THE TRANSONIC BUMP FOR Pushbutton CFD (ABOVE) AND OpenFOAM (BELOW) AT FREESTREAM MACH NUMBER of 0.675.

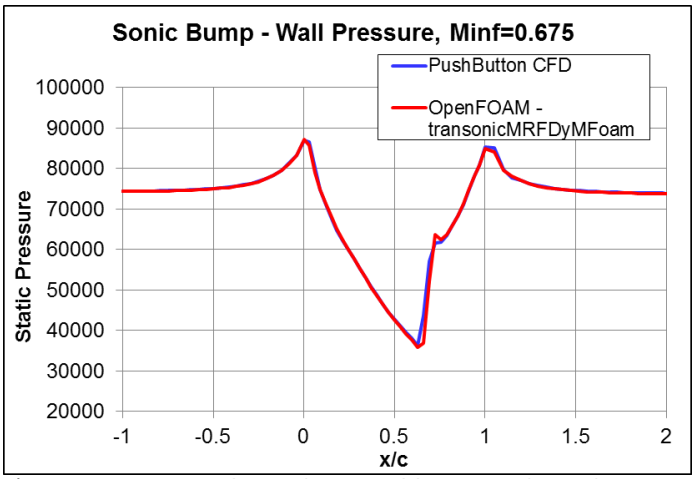

Figure 4. EULER SURFACE PRESSURE PLOT FOR THE TRANSONIC BUMP FOR PushButton CFD AND OpenFOAM.

More detailed data demonstrating more complex flow phenomena for the transonic bump was taken by Bashalo *et al.* (14, 15). The studies focused on turbulent flow separation behind the shock. Free stream Mach numbers above 0.85 showed the onset of separation behind the shock while values below were more or less free from any larger scale separation regions. Figure 5 shows the pressure coefficient values on the surface from viscous solutions using the SST turbulence model. While the comparison to data was reasonable for both solvers, it's important to note that the data were specifically taken in the range where the flow showed very nonlinear behavior. Certain inputs such as surface roughness, transition locations, and inflow turbulent energy, which could potentially affect the results, were not all available.

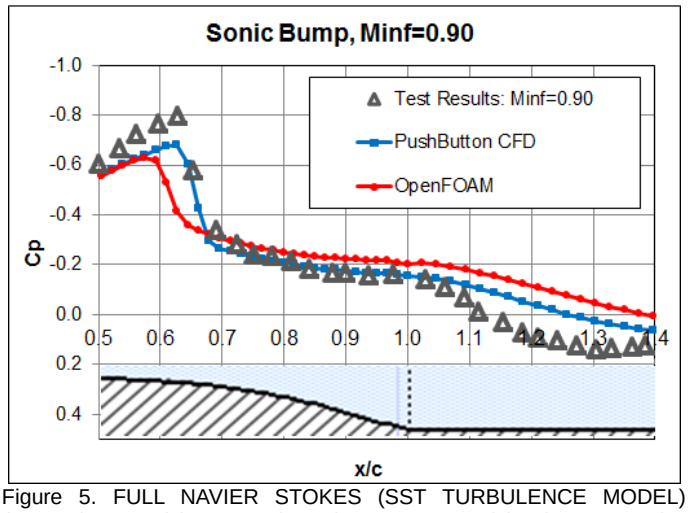

Figure 5. FULL NAVIER STOKES (SST TURBULENCE MODEL) SURFACE PRESSURE PLOT FOR THE TRANSONIC BUMP FOR Pushbutton CFD, OpenFOAM, AND TEST.

MAN AXIAL COMPRESSOR CASCADE

The MAN GHH_1-S1compressor cascade was a well-designed test series for a controlled diffusion axial compressor cascade published in the early to middle 1990's (16, 17). Most test data was taken at an AVDR of 0.9.

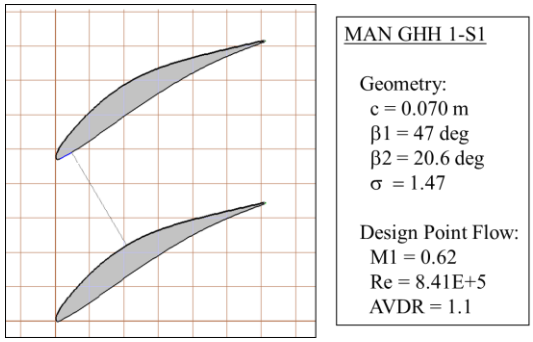

Figure 6. PROFILE SHAPE AND KEY PARAMETERS FOR THE MAN COMPRESSOR CASCADE.

A grid resolution study was conducted on both solvers using a Spalart-Allmaras (SA) turbulence model. The results, shown in Figure 7, show a very significant disparity in calculated loss as a function of Y+ with the results matching only at the lowest values. Close inspection of the source code revealed that the wall functions are not implemented in the SA model by default in OpenFOAM where as they are in most other turbulence models. For this reason, all results for the MAN cascade were generated on grids resolved down to the viscous sub-layer Y+~10. All subsequent cases covered in this work used a different turbulence model which implemented a wall function. Figure 8 shows the virtually identical results for the low Y+ grid.

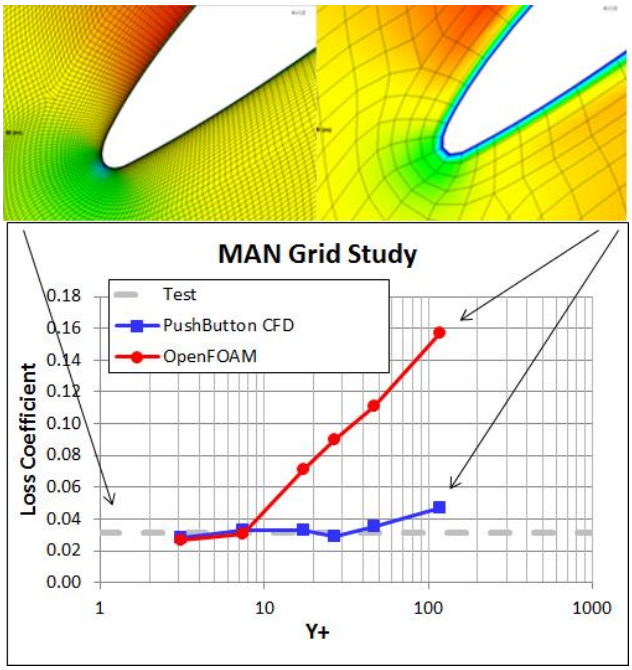

Figure 7. LOSS COEFFICIENT FOR THE MAN COMPRESSOR CASCADE AS A FUNCTION OF AVERAGE Y+ VALUES USING THE SPALART-ALLMARAS TURBULENCE MODEL.

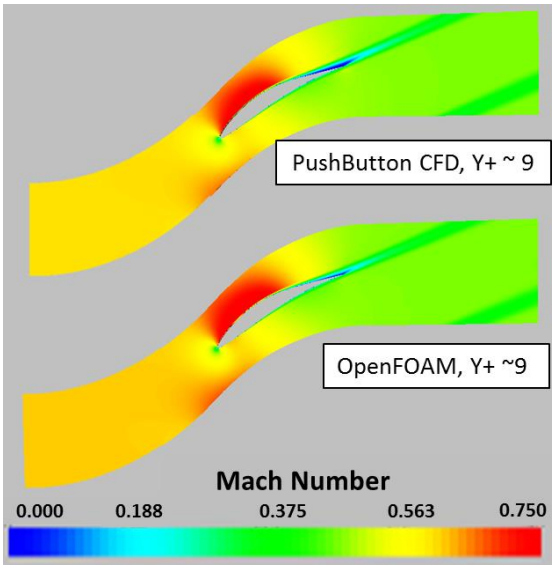

Figure 8. MACH NUMBER DISTRIBUTIONS FOR LOW Y+ SOLUTIONS FROM Pushbutton CFD (ABOVE) AND OpenFOAM (BELOW). NO WALL FUNCTIONS REQUIRED.

Results for loss coefficient (total pressure based) as a function of inflow Mach number is shown in Figure 9 for two incidence angles. The left hand results (shown in blue) are for a negative incidence condition and the right hand results (shown in orange) are for near zero incidence. Both solvers show excellent comparison to test data with just a small error in the low incidence choke prediction from the test. Interestingly, both solvers showed a virtually identical choke result.

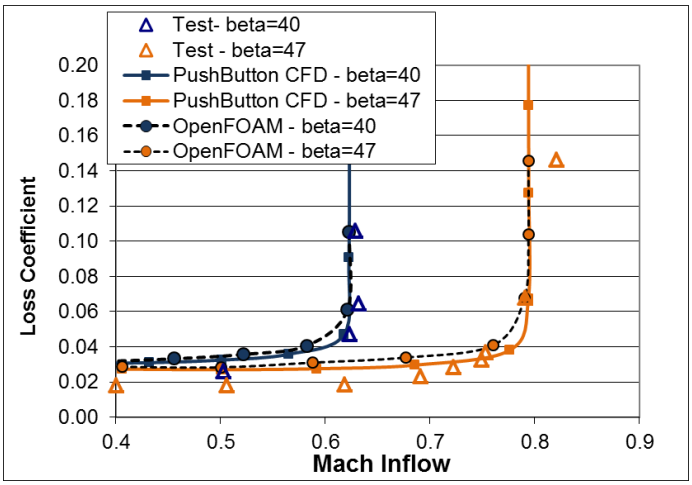

Figure 9. LOSS COEFFICIENTS AS A FUNCTION OF INFLOW MACH NUBER FOR A NEGATIVE INCIDENCE FLOW (BLACK LINES) AND ZERO INCIDENCE FLOW (YELLOW LINES).

Plots of isentropic Mach number for near zero incidence (Figure 10) and negative incidence (Figure 11) are shown below. Both are predicting very close agreement with the test results with the OpenFOAM result perhaps a bit closer on the negative incidence case.

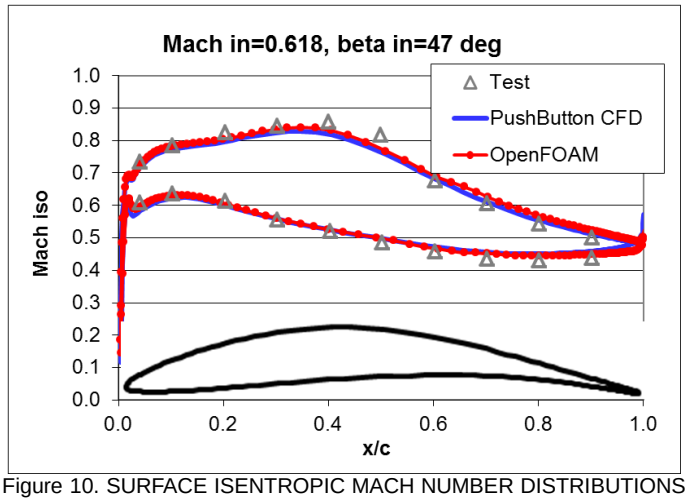

Figure 10. SURFACE ISENTROPIC MACH NUMBER DISTRIBUTIONS FOR THE MAN COMPRESSOR CASCADE AT NEAR ZERO INCIDENCE.

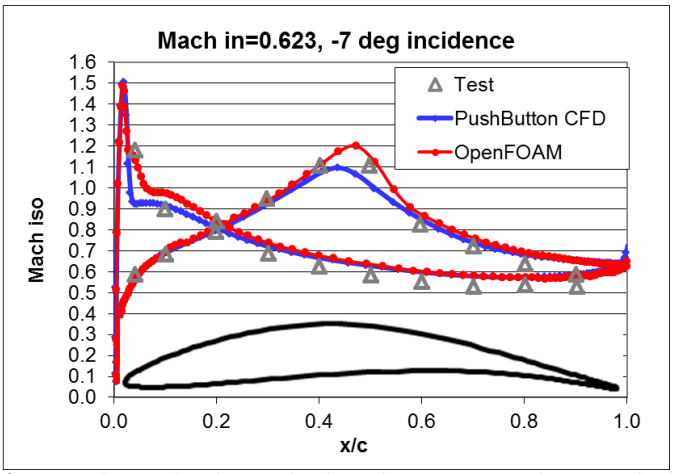

Figure 11. SURFACE ISENTROPIC MACH NUMBER DISTRIBUTIONS FOR THE MAN COMPRESSOR CASCADE AT NEGATIVE INCIDENCE.

VKI AXIAL TURBINE CASCADE

The VKI turbine test was published by Arts *et al*. in the early 1990's (18, 19). The cascade was a highly loaded turbine guide vane design for transonic to moderately supersonic flow. The shape of the cross section and some geometric parameters are shown below in Figure 12.

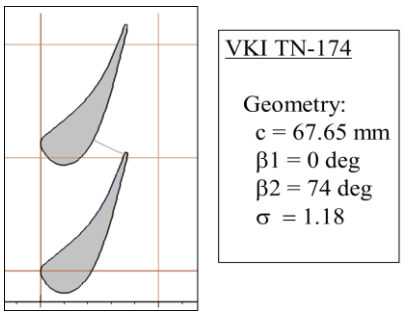

Figure 12. PROFILE SHAPE AND KEY PARAMETERS FOR THE VKI TURBINE CASCADE.

The results of kinetic energy based loss coefficient as a function of grid resolution for the k-ε turbulence model are shown in Figure 13. Note the much more limited sensitivity to Y+ with the wall function enabled k-ε model in OpenFOAM as opposed to the previous SA result. OpenFOAM shows an inflection in the loss curve which is perhaps related to details of implementation of the wall functions. All subsequent results for the VKI cascade were generated using a grid producing Y+ values of approximately 20. Figure 14 shows the Mach number distribution comparison between Pushbutton CFD and OpenFOAM for a super-sonic exit condition.

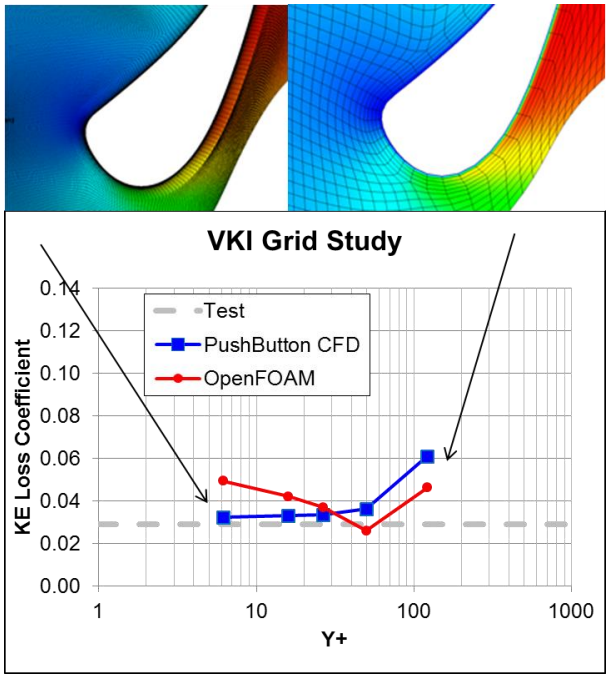

Figure 13. LOSS COEFFICIENT AS A FUNCTION OF AVERAGE Y+ FOR THE VKI TURBINE CASCADE. RESULTS FOR THE k-ε TURBULENCE MODEL WHERE WALL FUNCTIONS ARE INCLUDED IN BOTH SOLVERS.

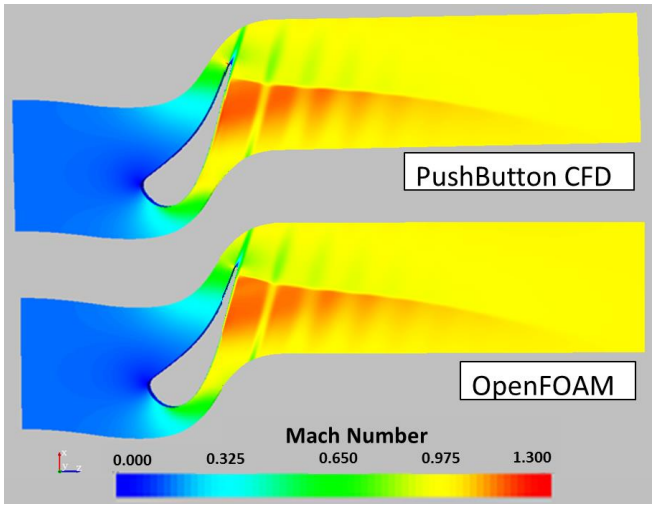

Figure 14. MACH NUMBER DISTRIBUTIONS FOR A SUPERSONIC EXIT CONDITION OF THE VKI TURBINE CASCADE.

Surface pressures are shown in Figure 15. Again, both solvers produce very good comparison to the test results and again, both solvers show virtually identical results where they deviate slightly from the test at the latter end of the suction side. Presumably, there is a small separation in the test that both solvers failed to pick up, most likely due to an inherent limit in the k-ε model.

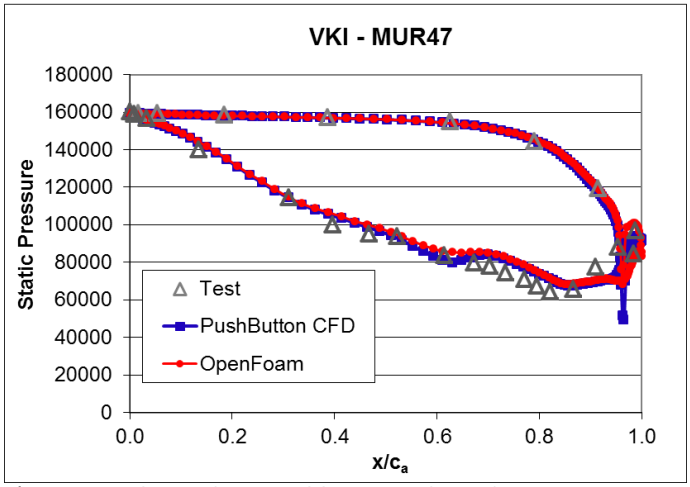

Figure 15. SURFACE PRESSURE PLOT FOR VKI TURBINE CASCADE.

Plots of loss coefficient and flow turning angle are shown in Figures 16 and 17. Despite the fact that loss is significantly more difficult to predict than flow quantities such as pressure or velocity, the results show reasonable agreement with the test data. Some of the discrepancy is certainly attributable to the fact that the test has a boundary layer transition point, somewhat past the leading edge, which generated lower losses in that region. Both solvers were run fully turbulent with no transition model and hence a slightly higher overall loss level. Results for flow turning are more or less within one degree from the test across the flow range.

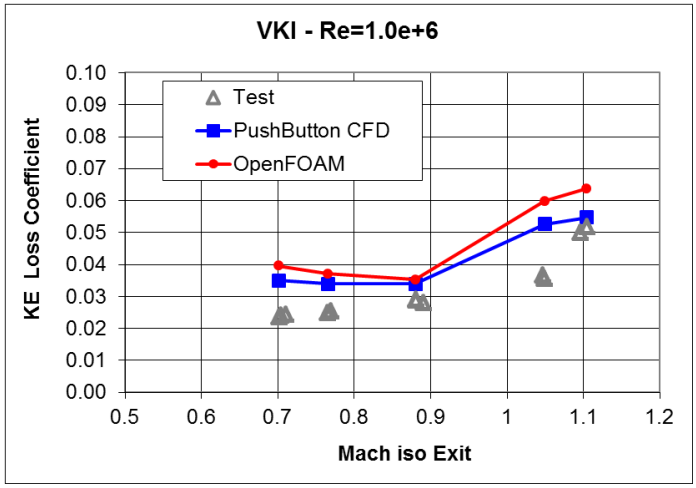

Figure 16. LOSS COEFFICIENT AS A FUNCTION OF ISENTROPIC EXIT MACH NUBER FOR THE VKI PROFILE.

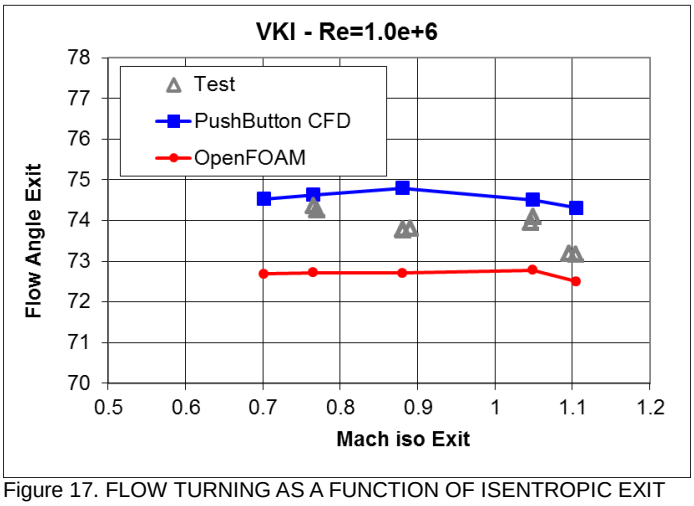

Figure 17. FLOW TURNING AS A FUNCTION OF ISENTROPIC EXIT MACH NUMBER FOR THE VKI PROFILE.

HODSON THREE-DIMENSIONAL AXIAL TURBINE CASCADE

The Hodson turbine cascade (20, 21) was an essentially two-dimensional turbine blade cascade geometry which generated a complex three-dimensional flow field from high turning of the non-uniform inflow. Figure 18 shows some basic geometry and flow information of the test. The grid consisted of 2.1M nodes with 91 points in the hub-to-shroud direction. The Y+ averaged about 21 and the k-ε turbulence model was used.

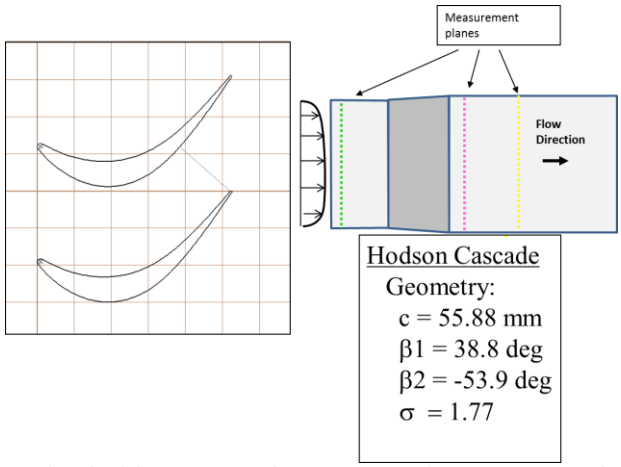

Figure 18. HODSON TURBINE SETUP AND FLOW PARAMETERS.

Figure 19 below gives an idea of the complex, three-dimensional nature of the flow formed by the secondary flows as calculated by Pushbutton CFD (left) and OpenFOAM (right). The isentropic Mach number distribution at mid-span is shown in Figure 20. Similar to the VKI turbine, there is very close agreement between both solvers and the test results although they both differ somewhat from the test at the suction side. Once again, the difference can probably be attributed to the failure of the turbulence model (k-ε in this case) to pick up the small separation region.

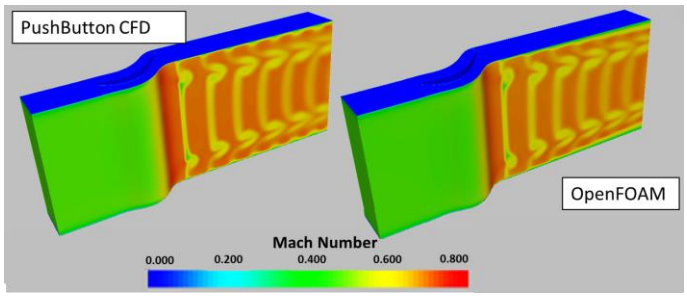

Figure 19. MACH NUMBER DISTRIBUTION SHOWING THE COMPLEX THREE-DIMENSIONAL FLOW FIELD IN THE HODSON TURBINE CASCADE.

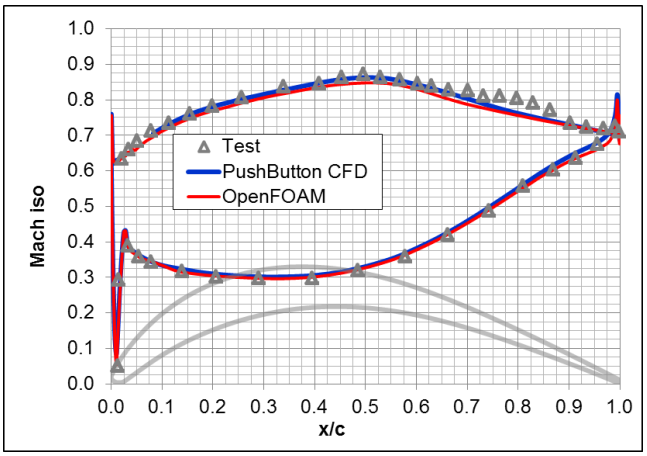

Figure 20. MID-SPAN ISENTROPIC MACH NUMBER DISTRIBUTION FOR THE HODSON TURBINE CASCADE.

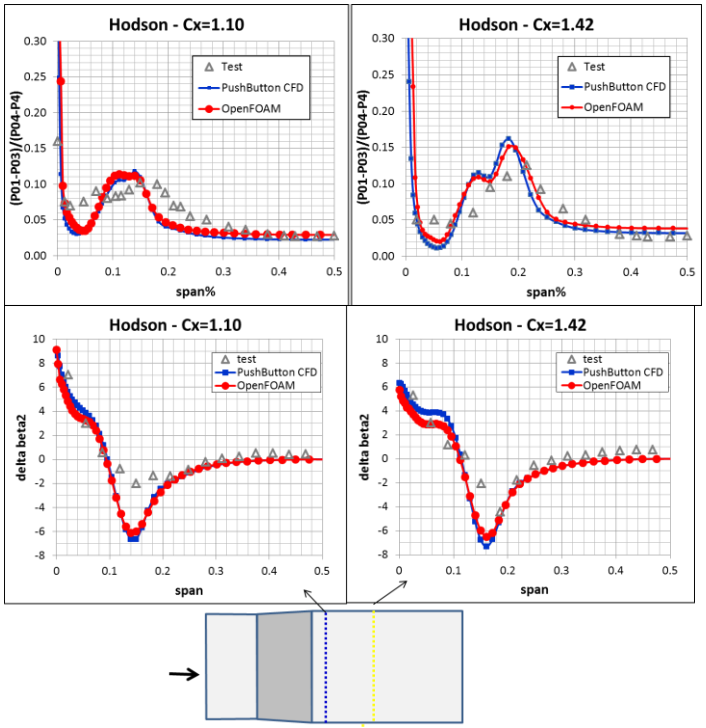

Figure 21. PITCH-WISE AVERAGED TOTAL PRESSURE LOSS (TOP) AND DEVIATION ANGLE (BOTTOM) AS A FUNCTION OF SPAN FOR TWO DOWNSTREAM LOCATIONS FOR THE HODSON TURBINE.

Plots of pitchwise averaged results as a function of span are shown in Figure 21 above. Loss is shown on top and flow turning angle on the bottom for two locations, one immediately down-stream of the trailing edge (left) and one at about 42% of axial chord downstream of the trailing edge (right). It's unclear what the source of the two peaks are in the upper right hand plot but both solvers pick it up. Perhaps the test sampling was too coarse to capture the effect. In general, very similar results are seen with respectable agreement with the test data and very close agreement between the two solvers.

ECKARDT-O RADIAL COMPRESSOR

The Eckardt-O compressor was a large scale radial compressor tested with extensive velocimeter data (22-26). The design had no splitters and used no back sweep at the exit so a significant jet-wake structure was formed due to high end loading of the impeller. A long tapering vaneless diffuser was used in the stage. A figure of the stage is shown in Figure 22. Besides the detailed laser velocimeter data, a significant amount of overall stage performance data makes it one of the best documented radial compressor tests available.

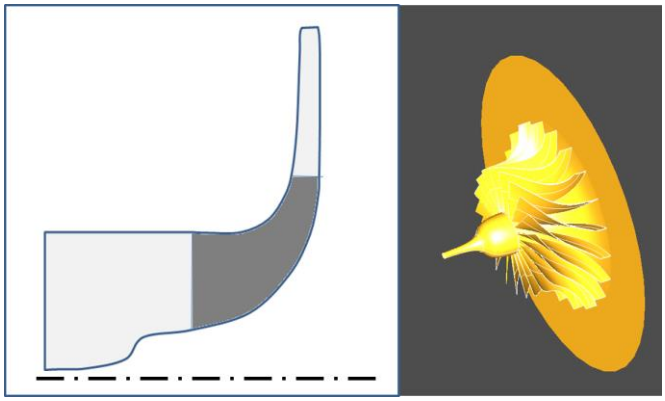

Figure 22. ECKARDT-O RADIAL COMPRESSOR STAGE.

The computational grid had 457K grid nodes. The SST turbulence model was used and the Y+ distribution averaged about 35 across the solutions. Figure 23 shows a plot of total-to-total pressure ratio for the stage for three separate speed lines. The results for the two solvers and test are in almost exact agreement, save for a significant inflection in the test results for the highest speed line. Normally, such an inflection is indicative of the onset of flow separation, most likely a shock/boundary layer interaction since the relative Mach number at the leading edge tip is supersonic for this speed line. Both solvers were run as far as possible to into the low flow regime until the convergence criteria was no longer meet.

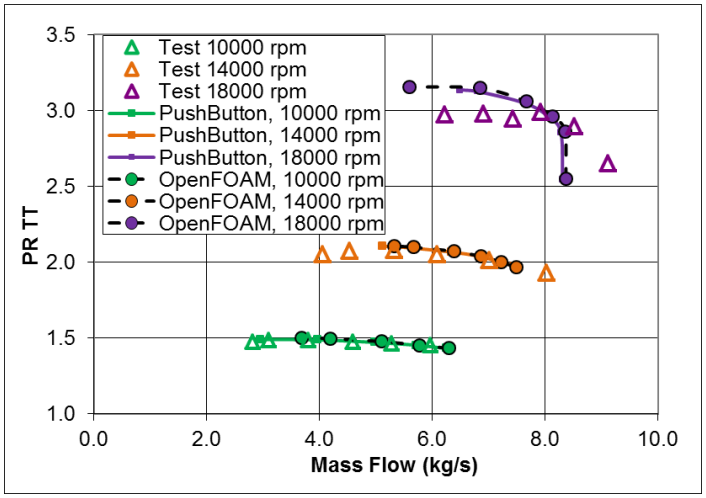

Figure 23. TOTAL-TO-TOTAL PRESSURE RATIOS FOR THREE SPEED LINES OF THE ECKARDT-O COMPRESSOR STAGE.

Plots of total-to-total efficiency are shown in the Figure 24. The plot is admittedly complicated, with nine lines in total, but it does show quite nicely the ability to capture the stage losses across the entire range of the machine. With the already mentioned exception of the highest speed line, the results for efficiency are generally within one point of the test with OpenFOAM showing a slight over prediction and Pushbutton, a slight under prediction of efficiency.

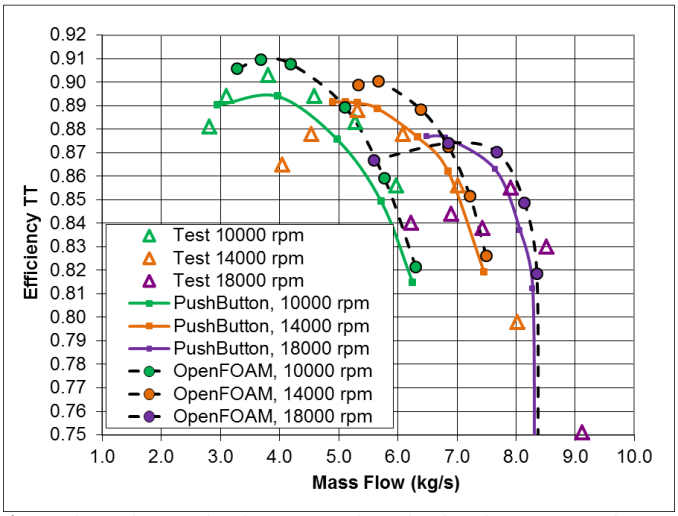

Figure 24. TOTAL-TO-TOTAL EFFICIENCIES FOR THREE SPEED LINES OF THE ECKARDT-O COMPRESSOR STAGE.

CCN-66 RADIAL COMPRESSOR

The CCN-66 stage (27) is a radial compressor with no splitters and a long pinched vaneless diffuser. A figure of the compressor is shown in Figure 25. The case used a lower grid density (264K nodes) and subsequently higher Y+ value averaging around 90 for the various solutions generated.

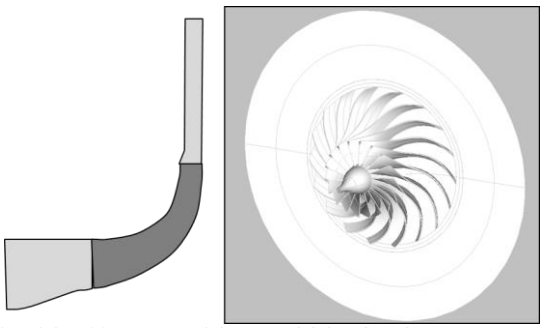

Figure 25. CCN-66 RADIAL COMPRESSOR STAGE.

Results for total-to-static pressure ratios are shown for three speed lines in Figure 26. The results show excellent agreement across the entire range for both solvers for all speed lines. Plots of total-to-static efficiency for the stage are shown in Figure 27. The results show very nice agreement with the test data, generally within a point of the test, for all three speed lines across the entire flow range of the compressor.

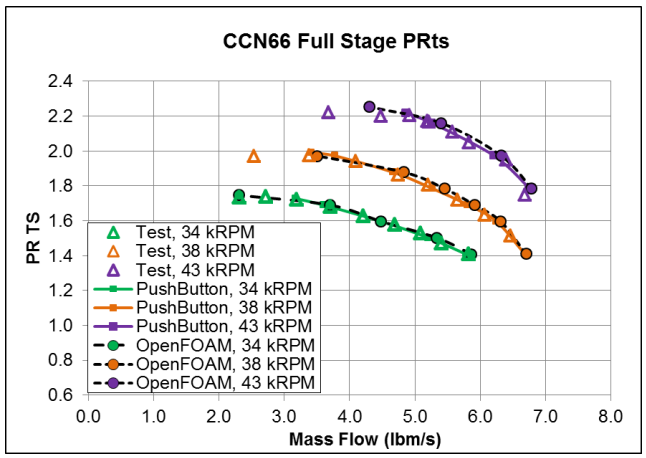

Figure 26. TOTAL-TO-STATIC PRESSURE RATIOS FOR THREE SPEED LINES FOR THE CCN-66 COMPRESSOR.

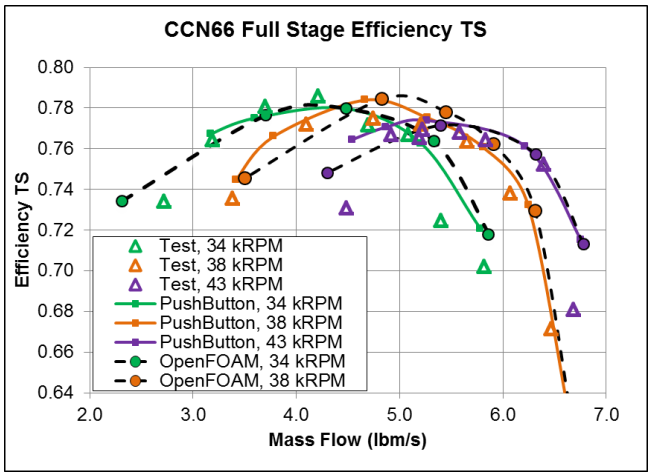

Figure 27. TOTAL-TO-STATIC EFFICIENCY LINES FOR THE CCN-66 COMPRESSOR.

RICARDO R70B RADIAL TURBINE

The last fully three-dimensional stage shown is that of a radial turbine published by Ricardo corporation in the 1950's and 1960's (28-30). CFD was run on the impeller alone (since a mixing plane option was not yet implemented) and the results corrected for full stage performance. Since nozzle performance was specifically measured, the corrections can be made with a high degree of confidence. Figure 28 below shows the turbine stage. The SST turbulence model used and the 100K node gird size provided an average Y+ distribution of approximately 20.

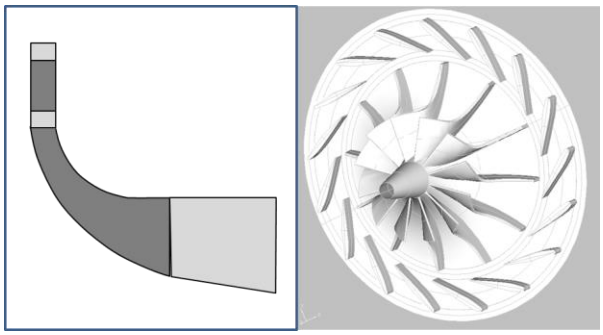

Figure 28. RICARDO R70B RADIAL TURBINE.

Results for the stage efficiency as a function of U/C_t (tip speed divided by isentropic expanded velocity) is shown in Figure 29. Both solvers predict the stage efficiency to within a point across a very significant flow range.

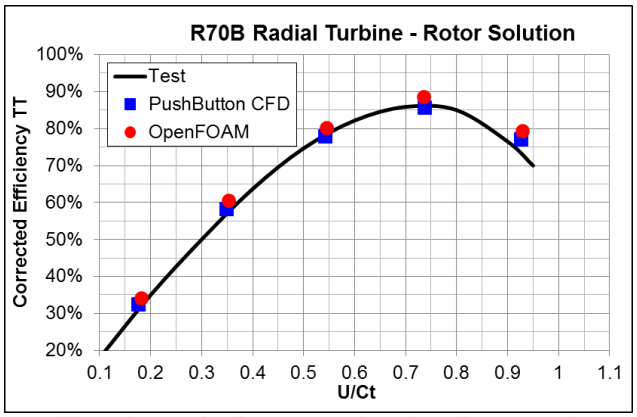

Figure 29. TOTAL-TO-TOTAL EFFICIENCY CURVE FOR THE RICARDO R70B RADIAL TURBINE.

RUN TIME

Run times for the density-based solver of OpenFOAM were considerably longer than for Pushbutton CFD or any other comparable commercial solver. The results were considered converged when the global mass flow showed no fluctuations outside a range of 0.1% of the final result. Figure 30 shows the run times for four OpenFOAM solutions run to convergence and normalized by the corresponding Pushbutton CFD run times. The results show a factor of ten times longer run times on average.

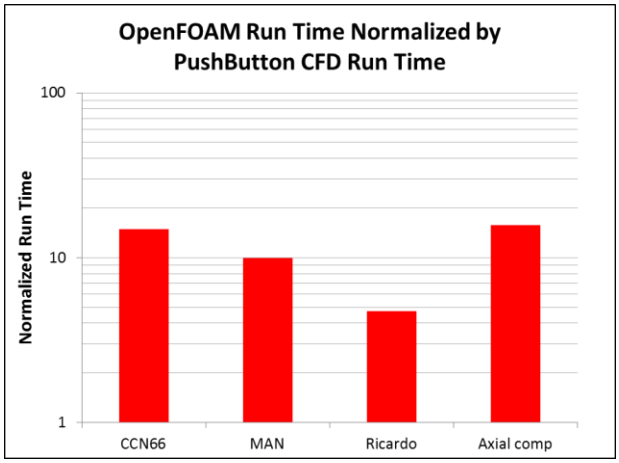

Figure 30. OpenFOAM RUN TIMES NORMALIZED BY Pushbutton CFD RUN TIME.

Investigation of the source code showed that two common acceleration methods, implicit residual smoothing and multigrid, are not implemented in this version of the solver. Pushbutton CFD uses both of these methods. Turning these options off in Pushbutton showed a very comparable level of run times for both solvers, shown in Figure 31. From this comparison, we can conclude that the OpenFOAM solver could probably be accelerated to comparable run time with the addition of these two acceleration techniques.

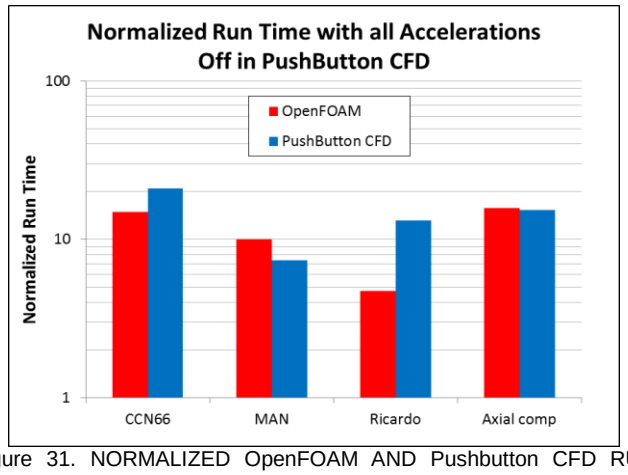

Figure 31. NORMALIZED OpenFOAM AND Pushbutton CFD RUN WITH ACCELERATION METHODS TURNED OFF.

An implementation of an implicit residual smoothing method (31) was applied to the solver and the results, shown below in Figure 32, show about a factor of two speed-up. The addition of a multigrid option is under way.

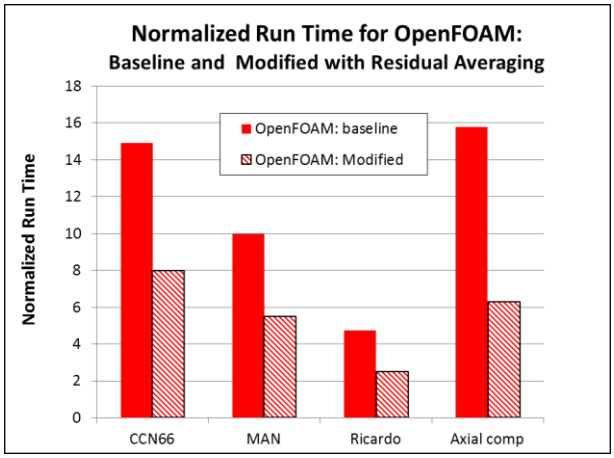

Figure 32. NORMALIZED OpenFOAM RUN TIMES FOR THE OpenFOAM BASELINE SOLVER AND ONE MODIFIED WITH RESIDUAL AVERAGING.

CONCLUSION

The sum total of results show that the density based solver of OpenFOAM is very effective in capturing not only the general flow characteristics in turbomachinery but the loss generation across a range of various designs with compressible flow. Where the results deviated from the test data, they showed very similar trends to the widely used commercial Pushbutton CFD code. This indicates the differences in results are due to the inherent limits of the turbulence models, grid resolution, or in the accuracy (or interpretation) of test results rather than any specific deficiency in the solver.

It is important to note that the results shown in this paper are only relevant for the density based solver *transonicMRFDyMFoam* (or one of the similar solvers included in the parent project (5)) and cannot be assumed to be representative of any of the other OpenFOAM solvers. In fact, the results presented at the beginning of the paper clearly indicate that other OpenFOAM solvers (almost all them pressure based) are not sufficient to capture higher Mach number flows even if they are modified for variable density.

Runs times for the density-based solver were much longer (by about a factor of ten) compared to typical times one would expect in most commercial solvers. Modification of the solver to accommodate residual averaging increased the speed of OpenFOAM by about a factor of two. The additional adoption of a multigrid capability should further increase the speed to a level comparable to other commercial solvers.

NOMENCLATURE

β_1- leading edge angle
β_2- trailing edge angle
σ - solidity
AVDR - Axial velocity density ratio
C_t – Velocity isentropically expanded to exit condition
c - chord
M- Mach number
Re - Reynolds number (chord based)
U – Turbine rotor tip speed

Subscripts

1- Leading edge or upstream
2- Trailing edge or downstream

REFERENCES

[1] Weller, H., Tabor, G., Jasak, H., Fureby, C., "A tensorial approach to continuum mechanics using object oriented techniques", Computers in Physics, vol. 12, pp. 620–631, 1998

[2] Fureby, C., Gosman, A., Tabor, G., Weller, H. Sandham, N., and Wolfsthein, M., "Large eddy simulation of turbulent channel flows", Proceedings of Turbulent Shear Flows 11, Vol. 3, pages 28-13, 1997

[3] Jasak, H., OpenFOAM: Future Developments, 1st OpenFOAM Workshop, Zagreb, Croatia, 2005

[4] Jasak, H., "OpenFOAM: a year in review", 5th OpenFOAM Workshop, Gothenburg, Sweden, June, 2010

[5] Borm, O. and Jemcov, A., "Density based Navier-Stokes solver for transonic flows", 6th OpenFOAM Workshop, Penn State University, June 2011

[6] Born, O., Kau, H., "Unsteady aerodynamics of a centrifugal compressor stage – validation of two different CFD solvers" ASME Turbo Expo 2012, GT2012-69636

[7] Blaim, F., Borm, O., Kau, H.P., "Implementation of rotor-stator interfaces in OpenFOAM", OpenFOAM Workshop, June 2008

[8] Beaudoin, H., Jasak, H., "Development of a generalized grid interface for turbomachinery simulations with OpenFOAM", Open Source CFD International Conference, 2008

[9] Anderson, M., "Turbomachinery validation with a density based OpenFOAM solver", 7th OpenFOAM Workshop, Darmstadt, Germany, June 2012

[10] "Test cases for computation of internal flows in aero engine components", AGARD Advisory Report No. 275., 1990

[11] Anderson, M., "Optimization of turbomachinery–validation against experimental results", Current Trends in Design and Computation of Turbomachinery, Prague, 2009

[12] Anderson, M., Gu, F., MacLeod, P., "Application and validation of CFD in a turbomachinery design system," IMECE2003, Washington D. C., 2003

[13] Ni, R., "A multi-grid scheme for solving Euler Equations", AIAA Journal, Vol. 20, No. 11, 1982, AIAA 81-1025

[14] Bashalo, W., Modarress, D., Johnson, A., "Experiments on transonic turbulent and supersonic turbulent boundary layer separation", AIAA 77-47, 1977

[15] Bashalo, W, Johnson, A., "Transonic, turbulent boundary-layer separation generated on an axisymmetric flow model", AAIA Journal, Vol. 24 No. 3, March 1986

[16] Steinert, W., Eisenberg, B., Starken, H., "Design and testing of a controlled diffusion airfoil cascade for industrial axial flow compressor application", Journal of Turbomachinery, Vol. 113., 1991

[17] Steinert, W., Starken, H., "Off design transition and separation behavior of a CDA cascade", Journal of Turbomachinery, Vol. 118., 1996

[18] Arts, Lambert de Rouvroit, Rutherford, "Aero-thermal investigation of a highly loaded transonic linear turbine guide vane cascade", von Karman Institute TN-174, 1990

[19] Arts, Lambert de Rouvroit M., "Aero-thermal performance of a two-dimensional highly loaded transonic linear turbine guide vane: a test case cascade", Journal of Turbomachinery, Vol. 114, Jan 1992

[20] Hodson, H.P., Dominy, R.G., "Three dimensional flow in a low-pressure turbine cascade at its design condition", Journal of Turbomachinery, Vol. 109, April 1987

[21] Hodson H.P., Dominy, R.G., "Off design performance of a low-pressure turbine cascade", Journal of Turbomachinery, Vol. 109, April 1987

[22] Eckardt, D., 1976, Detailed flow investigations within a high-speed centrifugal compressor impeller", Journal of Fluids Engineering, Sept 1976.

[23] Eckardt, D., 1975, "Instantaneous measurements in the jet-wake discharge flow of a centrifugal compressor impeller", Journal of Engineering for Power, July 1975

[24] Eckardt, D, "Flow field analysis of radial and backswept centrifugal compressor impellers, Part 1: Flow measurements using a laser velocimeter", Performance Prediction of Centrifugal Pumps and Compressors, ASME 1980

[25] Schuster, P., Schmidt-Eisenlohr U., "Flow field analysis of radial and backswept centrifugal compressor impellers, Part 2: Comparison of potential flow calculation and measurements", Performance Prediction of Centrifugal Pumps and Compressors, ASME 1980

[26] Private Communication

[27] Concepts NREC internal report.

[28] "First report on aerodynamic performance tests on cold rig, M.I.R.A. radial inflow turbine", Engineering Report DP.6845, Ricardo & Co Engineers, Nov. 1962

[29] Hiett, Palmer, "D.I.G.T. radial inflow turbine, cold tests on turbine B, turbine A and turbine D", Engineering Report 1381, Ricardo & Co Engineers, Sept.1956

[30] Hiett, "D.I.G.T. radial inflow turbine, cold tests on turbine B, and turbine A and turbine D", Engineering Report 1412, Ricardo & Co Engineers, Dec. 1958

[31] Frink, N. T., Parikh, P., Pirzadeh, S., "A fast upwind solver for the Euler equations on three-dimensional unstructured grids," AIAA-91-0102, 1991.